THE ASTROPHYSICAL JOURNAL, 448:138–148, 1995 July 20

THE VERTICAL DISTRIBUTION AND KINEMATICS OF H I AND MASS MODELS OF THE GALACTIC DISK

SANGEETA MALHOTRA
Princeton University Observatory, Peyton Hall, Princeton, NJ 08544; san@astro.princeton.edu
Received 1994 October 11; accepted 1995 January 30

ABSTRACT

We present full modeling of tangent point emission of H I as seen in the 21 cm transition in the inner Galaxy. This is done in order to measure the scale height and velocity dispersion of H I as a function of Galactic radius. The scale height and the velocity dispersion are used to consider the vertical equilibrium of the gas and constraints on the forces acting to keep it in such an equilibrium.

Besides the scale height and velocity dispersion of H I, the rotation curve and the z-centroid of the atomic layer are also derived. The model used takes into account emission from a large path length along the line of sight, corresponding to an interval (ΔR) of typically 1 kpc or smaller in galactic radius; and is parameterized by the scale height of the gas, the centroid in z, the rotation velocity and the velocity dispersion. These parameters are assumed to be constant over the interval ΔR. This model is then fitted to the 21 cm surveys of Weaver & Williams, Bania & Lockman, and Kerr et al. to determine the best-fit parameters.

The terminal velocity values are found to be in good agreement with previous measurements. The velocity dispersion is constant with radius at the theoretically expected value of 9–10 km s^{-1}. The Gaussian scale height of the H I layer increases with Galactocentric radius. The centroid of the layer deviates significantly from $z = 0$. Apart from small local variations, the four quantities measured: terminal velocity V_T, velocity dispersion σ_v, scale height σ_z and the centroid z_0 show similar behavior in the first and the fourth quadrants.

On balancing the turbulent pressure support of the layer against the disk gravitational potential, we confirm that additional support is needed for the H I layer. The radial profile of the reduced midplane mass density is an exponential with a scale length of 3.3 ± 0.3 kpc. This picture is consistent with a constant mass-to-light ratio of the disk, and extra support for the H I layer. This extra support (not provided by the turbulent pressure) should be constant with radius in the inner Galaxy.

Subject headings: Galaxy: kinematics and dynamics — Galaxy: structure — radio lines: ISM

1. INTRODUCTION

The analysis of vertical distribution and kinematics of disks of galaxies can tell us about the local mass density in the disk, distinct from the integrated mass inside a radius, derived from a rotation curve (Oort 1932). H I is a particularly good tracer in our own Galaxy as well as other systems because of its ubiquity (giving a radial mass distribution), ease of observation, and near isothermal nature, and has been used to derive disk mass densities in our own as well as other galaxies (Rupen 1990; Knapp 1987; Merrifield 1992). In the simplest case one considers the turbulent pressure gradient of the gas balancing the gravitational force in the z-direction. But the atomic gas may be subject to other pressures, for example, magnetic, cosmic ray, or radiation pressure. The relative contributions of these are essentially unconstrained. The only place where the mass densities obtained from the analysis of H I vertical equilibrium can be verified with a similar analysis is the solar neighborhood, where the vertical distribution and kinematics of stars can give an independent measure of the midplane mass density (ρ_0) as well as surface density (Σ) of the disk.

Issues related to the vertical equilibrium and pressure support of the H I layer have been well explored (e.g., Kellman 1972; Jackson & Kellman 1974; Badhwar & Stephens 1977); but relative contributions of magnetic, radiative and turbulent pressures remain open to discussion. (cf: Boulares & Cox 1990; Lockman & Gehmen 1991 and references therein). This paper is an effort to determine the value of velocity dispersion of the atomic gas and its variation with the Galactic radius and height above the plane and to determine the turbulent pressure that supports the gas.

As a starting point for this study we measure *both* the scale height and the velocity dispersion of H I as a function of Galactic radius between the radii of $\simeq 3$–8 kpc. The interpretation of kinematics of gas in the Galaxy is complicated due to our embedded perspective. The ubiquity of 21 cm emission of H I, and severe blending in the low Galactic latitudes add to the difficulty (see Burton 1988, 1992 for reviews). On the other hand our Galaxy is the only three-dimensional system we can study, and study at a high resolution as well.

For some purposes, simplifying assumptions can be made for certain lines of sight. For example, Galactic rotation is expected to have negligible contribution to the velocity spread of the gas at high latitudes and toward the Galactic center and anticenter. The velocity dispersion of H I has been measured at these locations (Radhakrishnan & Sarma 1980, Kulkarni & Fich 1985; Lockman & Gehman 1991). In the inner Galaxy, the tangent points too lend themselves to analysis with fewer assumptions. In the first and the fourth quadrant emission at extreme velocity comes from an annulus that is tangential to the line of sight, so we know the distance to the tangent points and can derive the rotation curve of the Galaxy; after correcting for the velocity dispersion of the gas (Kwee et al. 1954; Schmidt 1957). Knowing the distance we can also convert the angular extent of the gas to scale height.

In this paper we carry out full modeling of the tangent point emission to derive the velocity dispersion at the tangent points.

We model the tangent points in two dimensions, latitude and velocity. The apparent latitude extent of gas gives an extra handle on the relative distance of any parcel of gas, assuming that the scale height varies slowly with Galactic radius. The model is parameterized by the rotational velocity, the velocity dispersion, the scale height and the z centroid of the gas layer. These parameters are measured independently for the tangent point gas at each longitude, allowing us to study their variation with Galactic radius. No prior knowledge of the rotation curve is assumed. The problem of velocity crowding is dealt with by considering emission from a long path length (~ 1 kpc) up to the tangent points. Similar modeling has been carried out for molecular gas (Malhotra 1994, hereafter Paper I). The modeling procedure is described in § 2.1.

This model is then fitted to the H I surveys of Weaver & Williams (1973, hereafter WW), Bania & Lockman (1984, hereafter BL), and Kerr et al. (1986, hereafter Parkes). The specifications and parameters of the surveys are briefly enumerated in § 2.2.

We try to estimate uncertainties on the derived parameters in § 2.4. The errors are not Gaussian, and are dominated by asymmetries and other systematic deviations from the simple model used here, with the atomic gas layer represented by a single Gaussian z-profile and a single velocity dispersion component. These uncertainties (and possible systematics) are estimated by changing the velocity and latitude ranges over which the fits are made.

The modeling of the data at every 1° in longitude yields the rotation curve, the scale height, and the velocity dispersion of H I as function of Galactic radius between 3–8 kpc, for both the first and the fourth quadrant. Section 3 describes the resulting best-fit estimates, and some possible implications for Galactic structure. One of the objectives of this study is to examine the vertical equilibrium of the gas. The parameters derived here are used to do so using the thin H I–layer approximation in § 4.1. In § 4.2 we consider a more realistic disk potential and calculate the expected z-profile for isothermal gas. We also estimate by how much the thin H I–layer approximation underestimates the midplane mass density.

2. METHOD

2.1. *Tangent Points*

Assuming a circularly symmetric model of the galaxy, we can obtain distances to the emission at extreme positive velocities in the first quadrant and extreme negative velocities in the fourth quadrant. At each Galactic longitude l, extreme velocity emission comes from the tangent point at a galactocentric radius of $R = R_0 |\sin l|$ (Fig. 1) and a distance $d = R_0 \cos l$ from the Sun. From the observed b extent and the terminal (extreme) velocities one could calculate the scale height ($z = R_0 \cos l \tan b$) and the rotation velocity. The velocity profiles do not have a sharp cutoff due to the velocity dispersion of the gas. Ideally the emission from the tangent point $T(b, v)$ is a bivariate Gaussian in altitude and velocity; but emission from nearby radii is not well separated in velocity because of the velocity dispersion of the gas.

The finite velocity dispersion has two main effects that the present analysis takes into account. First it makes the velocity-to-distance conversion fuzzy, so it is difficult to separate emission from R (at the tangent point) and that from $R'(R' = R + \Delta R)$, where ΔR depends on the velocity dispersion. For cold gas (zero velocity dispersion) a difference in velocity $\Delta V_T = 7$ km s^{-1} would correspond to $\Delta R \simeq 270/\sin(l)$ pc near the tangent point. While the radial interval is small the line-of-sight distance changes substantially, leading to velocity crowding (Burton 1971), so that $T(b, v)$ is no longer a simple bivariate Gaussian in v and b.

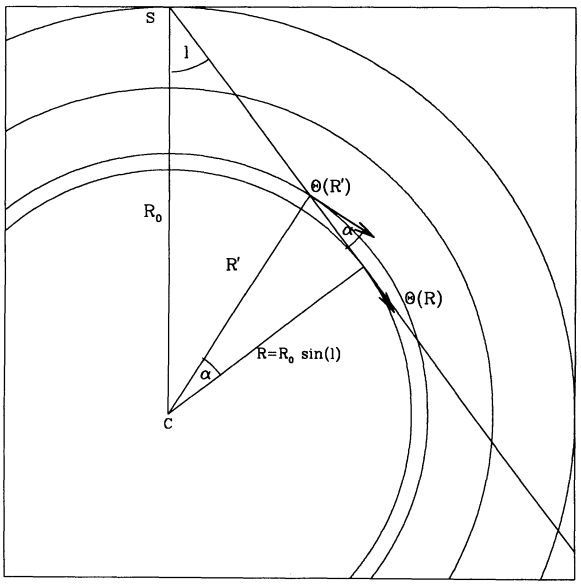

FIG. 1.—The geometry of the tangent point emission. S indicates the position of the Sun, R is the Galactic radius at the tangent point, and R′ is a subtangent point. The models of the tangent point emission take into account the emission from the annulus between R and R′.

Celnik et al. (1979) and Rohlfs & Kreitschmann (1988) derived the expression for the expected line shape near terminal velocity taking into account emission from gas all along the line of sight, and used it to identify tangent point emission. In this paper we calculate the two-dimensional (in latitude and velocity) contours of emission from near the tangent point, i.e., between R and $R + \Delta R$, assuming the scale height, rotation velocity Θ, and velocity dispersion to be constant over ΔR. The expected contours have a distinct shape at the tangent point (Fig. 2). The H I emission does not peak at the terminal velocity (line-of-sight velocity for the tangent point gas), but at a lower velocity.

Consider emission seen at velocities V close to the terminal velocity V_T; $(\Delta V = |V_T - V| \ll \Theta)$. This emission comes from gas at the annulus at radius R'. An observer's line of sight intersects the annulus at radius R' at two points (Fig. 1). The distances to the points of intersection, r_n and r_f are given by

$$r_{n,f} = R_0 \cos l \mp R' \sqrt{1 - \frac{\sin^2 l}{(R'/R_0)^2}}\,, \tag{1}$$

$$\Rightarrow r_{n,f} = R_0 \cos l \mp R_0 |\sin l| \sqrt{\frac{\Theta^2}{(\Theta - \Delta V)^2} - 1}\,. \tag{2}$$

For the same scale height, gas at the subtangent points will have smaller and larger latitude extent than the tangent point gas, corresponding to the far and the near part of the annulus R'. The apparent scale heights σ_{zn} and σ_{zf} at the near and far side of the annulus are given in terms of the scale height at the tangent point $\sigma_z(V_T)$ by the following relation.

$$\sigma_{zn,zf}(V) = \frac{\cos l}{\cos l \mp |\sin l| \sqrt{2\Delta V/\Theta}}\, \sigma_z(V_T)\,.$$

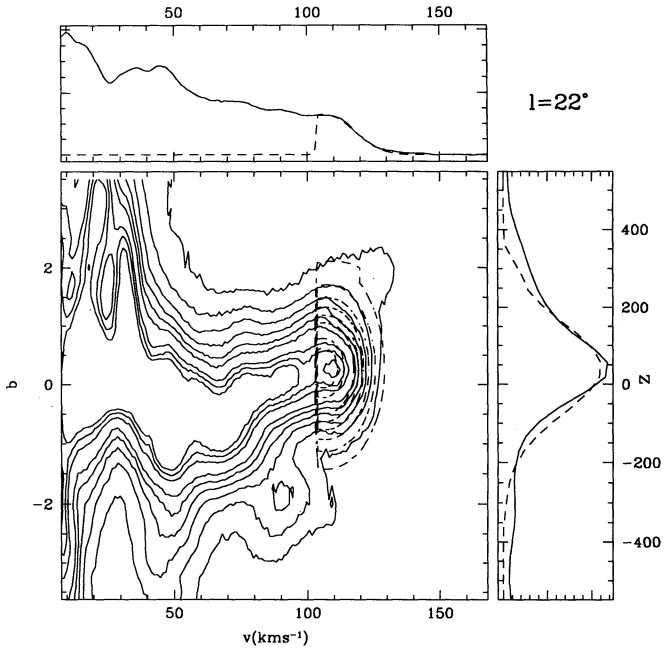

FIG. 2a

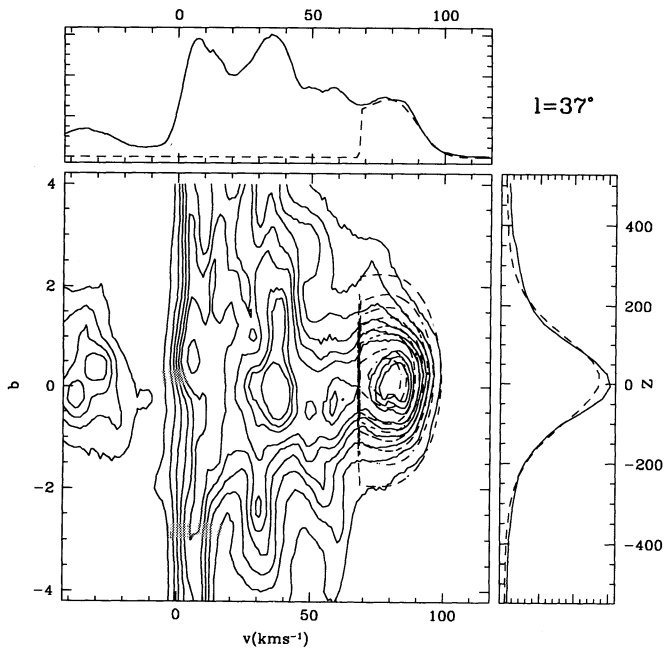

FIG. 2b

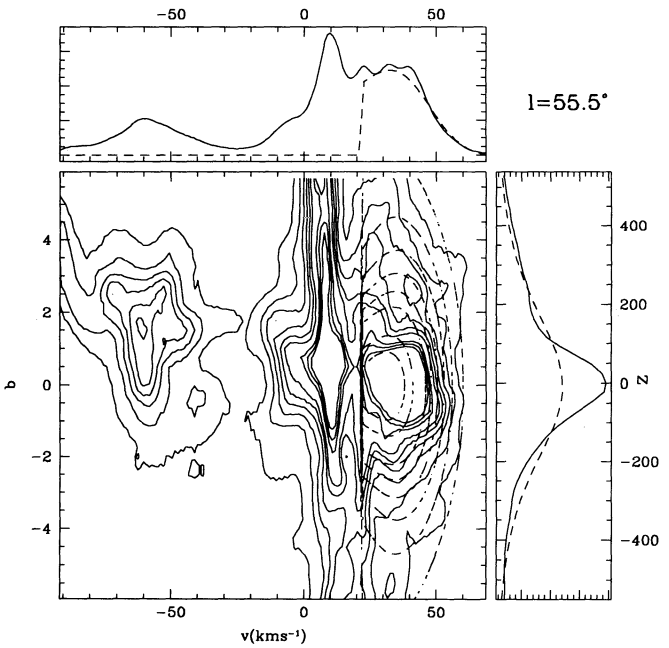

FIG. 2c

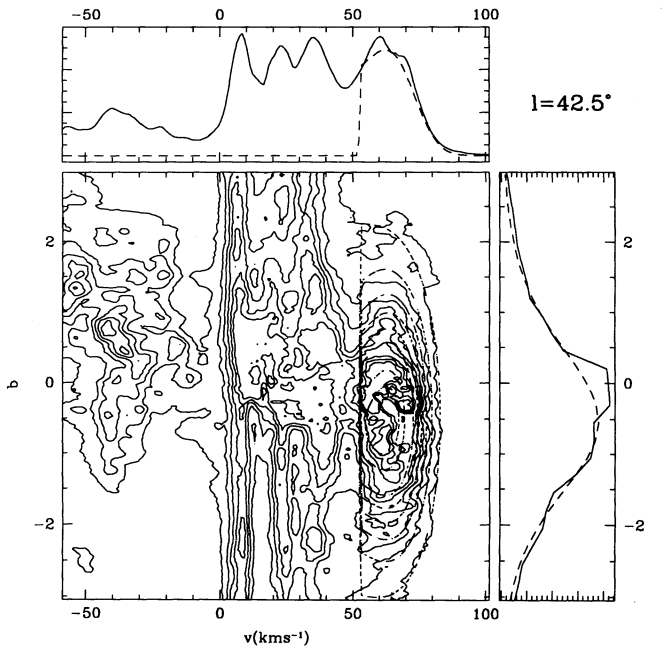

FIG. 2d

FIG. 2.—(*a–e*) Latitude-velocity maps of the 21 cm emission at the longitudes $l = 22°$, 37°, 55° (WW survey), 42°.5 (BL survey) and 290° (Parkes survey). The best-fit models to the tangent point emission are shown superposed on the data. Contour levels are defined at 10, 20, 30, ..., 90% of the peak temperature in the best-fit model. The model shows an abrupt cutoff at the velocity V_{crit}, because the fitting is done only for $V > V_{crit}$; V_{crit} being the velocity at which the tangent point emission is 80% of the peak value or chosen according to other criterion described in § 2.3.

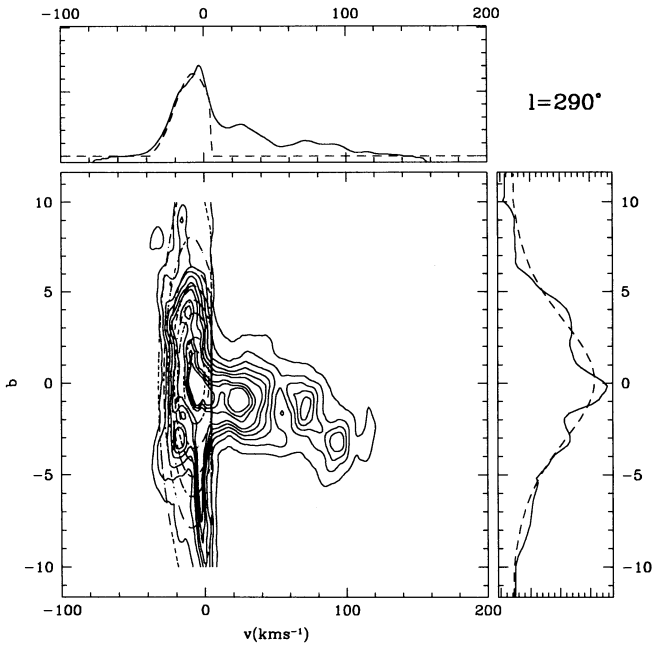

FIG. 2e

Taking into account velocity crowding effects, the optical depth per velocity interval is determined by the line of sight distance per unit velocity interval.

$$\frac{dr}{dV} = \frac{R_0 \Theta^2 \sin l}{[\Theta_0 \sin l + V(R')]^3} \left\{ \frac{\Theta^2}{[\Theta_0 \sin l + V(R')]^2} - 1 \right\}^{-1/2} . \quad (3)$$

Thus the column density of H I in the velocity interval ΔV (corresponding to $\Delta R = \Theta_0 / R_0 |\sin l|$) near the terminal velocity, keeping parameters, σ_v, σ_z fixed over the velocity interval is

$$N_H(b, v) = A \sum_{1,2} \int \frac{1}{2\pi\sigma_V \sigma_z(V)} \times \exp\left\{ -\frac{(v/\cos b - V)^2}{2\sigma_V^2} - \frac{[R_0 \cos l \tan b - z_0(V)]^2}{2\sigma_z(V)^2} \right\} \frac{dr}{dV} dV . \quad (4)$$

2.2. *Data*

The modeling is done for three H I surveys of the Galactic plane. The H I survey by Weaver & Williams (1973, hereafter WW) covers latitudes $b = -10°$ to $b = 10°$, sampling every $\Delta b = 0.^\circ 25$ with a beam width of 36′. The results from modeling this survey are compared to the results from an Arecibo H I survey (Bania & Lockman 1984, hereafter BL), done with a beam size of 4′, and latitude coverage $\pm 4°$. In the fourth quadrant we use the Parkes survey (Kerr et al. 1986). The beam width is 48′ and the latitude coverage $\pm 10°$. The resolution of these surveys is not insubstantial compared to the scale height of the gas. A half-power beam width of 18′ corresponds to linear scale of 40 pc at the tangent point at the longitude 20° and to 21 pc at longitude 60°. The Arecibo survey offers higher resolution, but smaller latitude and longitude coverage ($|b| < 4°$, $32° < l < 64°$). We will see that for the midplane position it will useful to compare the results from both the surveys.

The observed brightness temperatures are converted to H I column densities assuming a constant spin temperature $T_{spin} = 127$ K (Mihalas & Binney). The parameters (like scale height and velocity dispersion) derived were found to be insensitive to the exact (127 ± 10 K) value of the spin temperature. We derive parameters for the longitude range $20° < |l| < 62°$. The lower limit is to avoid the noncircular kinematics of the bar, and the upper one because this method becomes unreliable near the solar circle.

2.3. *Fitting*

The model profile is calculated (eq. [4]) as a function of latitude b and velocity v for each longitude and the best fit is determined by minimizing absolute differences between the model and the data. This perhaps is a more robust method than minimizing least-squares, given the higher-than-Gaussian tails expected in the z distribution (§ 4.1), and the expected presence of H I clouds, self-absorption, absorption, and asymmetries, all of which contribute to non-Gaussian noise. The minimization is done using an downhill simplex algorithm, "AMOEBA" (Press et al. 1993). In almost all the cases we are able to find reasonable fits to the data at the tangent points. Figure 2 shows some examples of fits from the three surveys. Best-fit models for all longitudes are published elsewhere (Malhotra 1994b) and are available from the author.

The velocity range over which the fit is made is determined by the width of the extreme velocity feature. For each line of sight the spectra at all latitudes are summed to form a composite spectrum. The peak at the highest velocity is identified as the terminal velocity feature. The lower velocity at which the emission drops to 80% of the peak value is defined as V_{crit}. We fitted the emission seen at velocities greater than V_{crit}.

The H I, because of its high-velocity dispersion and ubiquity, shows severe blending and it was not possible to isolate a single tangent point emission peak in a large number of the longitudes (for example, Fig. 2*b*). In that case it is not possible to identify V_{crit}, and the range over which the tangent point fitting is done; but we would like to restrict the range over which we fit parameters. We then identified the extreme (positive in the first quadrant and negative in the fourth) velocity at which the emission dropped to zero (or less than 3 times the antenna noise) as V_{ext} and then defined V_{crit} to satisfy the relation: $|V_{crit} - V_{ext}| = (14 + 26|\sin l|)$, the second term is used so that the velocity intervals correspond to the same interval in Galactocentric radius ($\simeq 1$ kpc).

In the next section we will see that the best-fit models obtained are not very sensitive to small ($\simeq 10$ km s^{-1}) change in the velocity range over which the fitting is done. To test this we do model-fitting for different values of V_{crit} for one of the longitude $l = 42°$. The results of this test are described in the next section, along with other tests for determining errors.

2.4. *Error Analysis*

The assumptions made in the modeling of the tangent point gas are as follows. We have assumed that the four parameters: the scale height, the velocity dispersion, the rotational velocity and the position of the centroid of the gas with respect to the $z = 0$ plane, remain constant over the radial range we fit over, which is no more than 1 kpc. So the parameters we obtain are averages over such a range in Galactocentric radius. While deriving the models we have also implicitly assumed that the

midplane volume density $n_{\rm H\,I}$ is not varying systematically over that region. Also, the spin temperature of the gas is assumed to be constant. We also assume circular motions, apart from velocity dispersions. But we know that $n_{\rm H\,I}$ varies on all scales, and we expect that $n_{\rm H\,I}$ and velocity fields undergo large-scale variations at the spiral arms.

An additional source of error is that the beam sizes for the WW and Parkes surveys are greater than 0°.5. Typical longitude intervals over which we make "independent" estimates and see the parameters change is 1°. What that means is that we are averaging over the azimuthal (longitudinal) extent of the beam, as well as the line-of-sight interval. While the latter is accounted for in the model (by changing the b-extent corresponding to the same scale height, for example), the former is not accounted for. Notice that the model fits are substantially better for the BL survey (Fig. 2*e*), where the resolution is better. The models, however, describe the gross features of the gas distribution fairly well, and the parameters derived from the BL survey agree with those from WW survey (see Figs. 5, 6, 7, 8 below).

We find that the chi-square per degree of freedom: χ^2/N, for the fits is almost always greater than 1. Moreover, looking at the residuals left after subtracting the model from the data, we find that the quality of fit is always dominated by systematic errors, for example, asymmetries in the b-extent about the centroid, high-than-Gaussian tails at high z, etc.

To test for systematic sources of error, we do the model fitting for different ranges in b, for two lines of sight $l = 35°$ and $l = 25°$. Figure 3 shows the best-fit parameters for the different z-ranges. The error bars on the parameters are estimated from dispersion in these best-fit values and are not formal error bars. The velocity dispersion is found to be uncertain by $\simeq 1$ km s^{-1}, the terminal velocity by $\simeq 2$ km s^{-1}, the midplane position by $\simeq$2–8 pc, and the scale height by $\simeq$15–20 pc.

The other noticeable effect is the variation of the parameters between $b > 0$ and $b < 0$. The scale height is larger on one side of the plane than the other. There is also no significant variation of velocity dispersion with distance from the plane. That the H I velocity dispersion does not change with height above the plane is a strong indication that the gas is isothermal.

We also test for the dependence of the best-fit parameters on the velocity range over which the fitting is done. Figure 4*b* shows the best-fit parameters plotted against the $V_{\rm crit}$ where the fitting starts. The variations in parameters are comparable to the uncertainties quoted in the last paragraph for three of the four parameters. The scale height σ_z, however, stays constant for small changes ($\Delta V_{\rm crit} < 10$ km s^{-1}) in the $V_{\rm crit}$; and shows a systematic rise as we decrease the $V_{\rm crit}$ to include emission from a larger part on the line-of-sight gas (Fig. 4*a*). This is reasonable, as we are including more gas along the line of sight in the average, and this gas, being at a larger Galactocentric radius, has a greater scale height.

The velocity interval between the terminal velocity of 71 km s^{-1} and the most extreme $V_{\rm crit} = 34$ km s^{-1} corresponds to $\Delta R \simeq 2$ kpc. In § 3 it is shown that the scale height increases by $\simeq$40 pc in that radial interval, and we see that the estimate of the average scale height increases by $\simeq$20 pc when we include gas from that annulus. So what if $V_{\rm crit}$ is too low and includes too large a range in ΔR? For small changes in $V_{\rm crit}$ (<10 km s^{-1}) the results are not very discrepant, and the test case in Figure 4*b* is an extreme example of low $V_{\rm crit}$. If a large systematic mistake is made in identifying the range of velocity to fit over for a large fraction of longitudes, we may be underestimating the increase of σ_z with Galactic radius.

3. RESULTS

3.1. *Midplane Z_0*

The position of the centroid of the H I layer deviates significantly from $Z = 0$, even in the inner Galaxy. Lockman (1977) has pointed out the large-scale Z-displacements of Population I objects in the inner Galaxy from the $Z = 0$ plane. For the inner Galaxy, the Z displacement can most reliably be measured at the tangent points. At other places we see a superposition of the near and far layers. The midplane positions Z_0 of the gas layer at the tangent points in the first and the fourth quadrants are shown in Figure 5. Also shown superposed are the midplane deviations of the molecular gas as measured by CO emission (Malhotra 1994; Bronfman et al. 1988).

The deviations of the molecular gas layers are easily detected because of the smaller scale height of the layer ($\simeq$50 pc compared to >100 pc for H I scale height), and because of the high resolution of the surveys (100″–7′.5). The WW and Parkes surveys have linear resolutions of several tens of parsecs depending on the longitude of the tangent point. The Z_0 values determined from BL survey with 9 times smaller beam size, agree well with those determined from WW survey (Fig. 5). This leads us to have confidence in Z_0 measured in the fourth quadrant also.

The midplane positions of the atomic and molecular gas show similar deviations from the $Z = 0$ plane, except at $l = 30°$–$37°$. In the first quadrant the maximum deviation in $Z_0 \simeq -50$ pc is at $\sim l = 42°$. Moreover, Z_0 seems to be mostly negative, changing sign at $l = 53°$. In the fourth quadrant the opposite is true. Most of the gas layer has a positive deviation from $Z = 0$, changing sign at $l = -55°$. Maximum excursion is $Z_0 \simeq 50$ pc at $l = 33°$. Recall that the outer galaxy warps to positive Z in the first quadrant, and negative Z in the fourth. Thus, the inner Galaxy displacements, although complicated, are largely opposite to the outer Galaxy warp.

3.2. *Scale Height*

The scale height is estimated by fitting a model which assumes a Gaussian profile for the vertical distribution of H I, with the midplane position Z_0 and scale height as parameters. An isothermal population tracing an external potential is expected to have a nearly Gaussian profile near the plane (see § 4.1 a treatment beyond this approximation). There are observations to indicate that there is more H I at higher Z (>500 pc) than predicted by a single Gaussian fit made near the plane (Lockman 1984). However, it is not possible to reliably estimate all the parameters required for a more complicated model, say with two scale heights and as many values of velocity dispersions. A single Gaussian profile in z describes $\sim$90% of the H I in the inner Galaxy (Lockman 1984).

As mentioned before, the beam widths in the Parkes and WW surveys are nonnegligible compared to the scale height. Moreover the beam widths correspond to larger physical sizes for tangent points at greater distances frpm the Sun (at small Galactic radii). The best-fit scale heights are corrected for this effect by subtracting the beam half-widths in quadrature. As seen in Figure 6, the scale height increases with Galactic radius, for $R > 0.5$–$0.6R_0$, in both the first and the fourth quadrant. The variation of the scale height with R is similar in the two quadrants. H I in external edge-on galaxies also show increase in scale height with radius (Rupen 1990).

In the first quadrant the BL and the WW data show the same scale heights (after correction for beam size) for longitudes $l \leq 48°.6$. For higher longitudes the BL survey show a

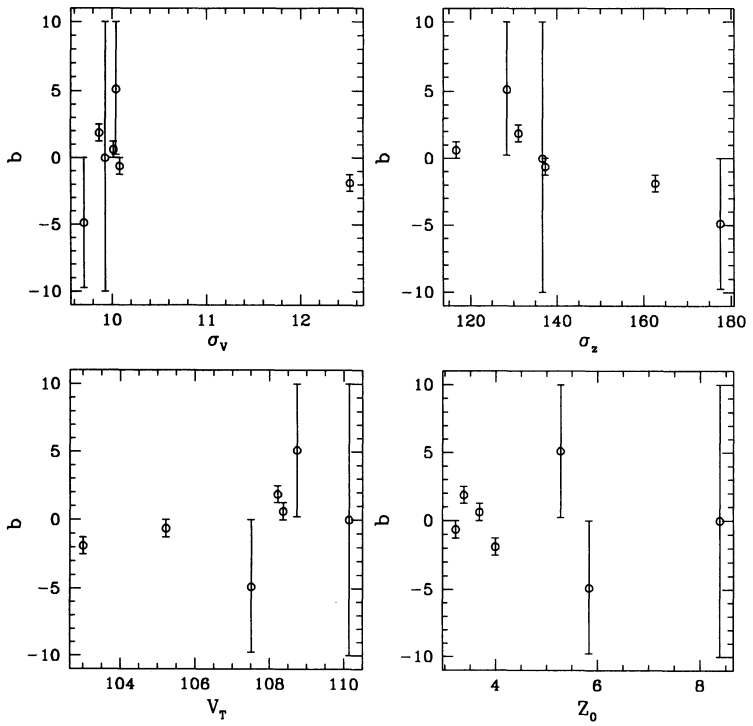

FIG. 3*a*

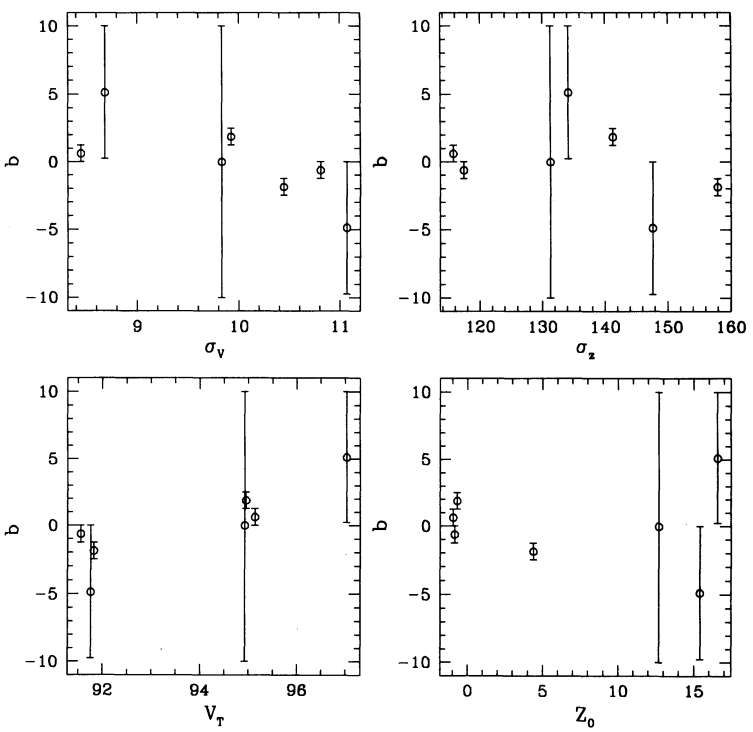

FIG. 3*b*

FIG. 3.—The effect of changing the *b*-range over which the fitting is done for the longitude (*a*) $l = 25°$ and (*b*) 35°. The latitude range is plotted on the *y*-axis, and the vertical bars indicate the *b*-range over which the fitting was done. The parameters (with the exception of scale height σ_z) are fairly insensitive to the *b*-range of the fit. The scale height is different on the north and the south side, ranging from 120 pc in the north to 180 pc in the south. The small midplane displacement to the north does not fully account for this. This shows that the layer is fairly asymmetric.

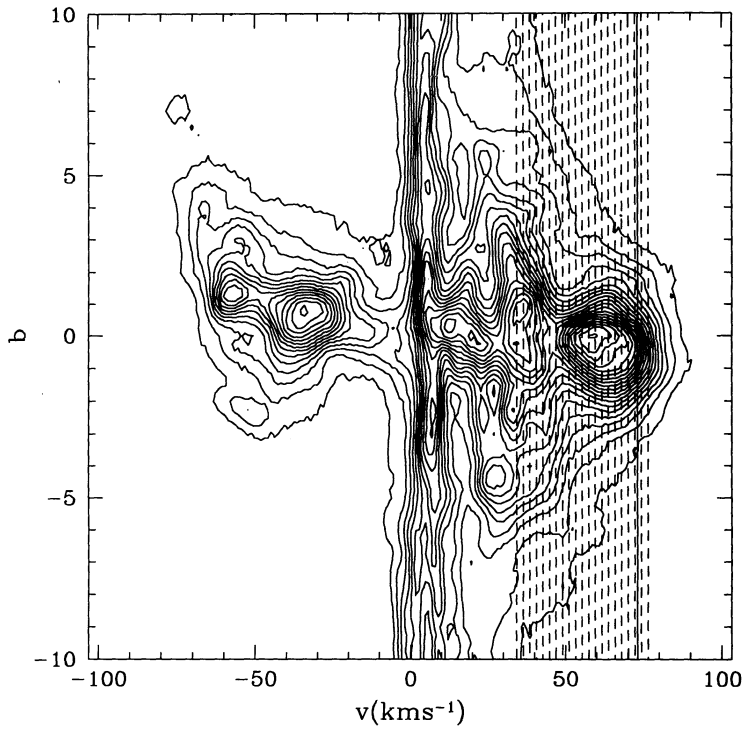

FIG. 4a

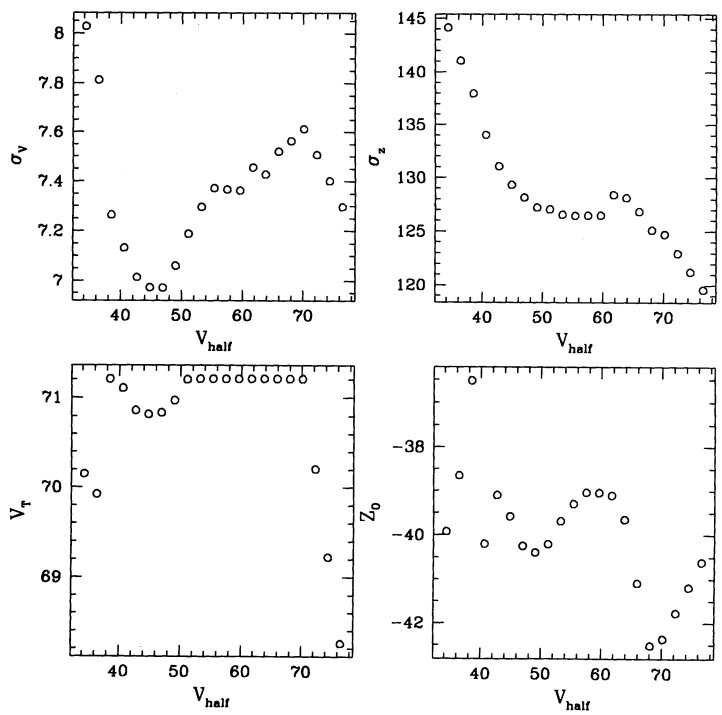

FIG. 4b

FIG. 4.—Latitude-velocity maps of 21 cm emission of H I at the longitude $l = 42°$. The dotted vertical lines show the various values of V_{crit}. The fitting is done for emission at velocities $V > V_{crit}$. The solid line shows the tangent point velocity and is not coincident with the peak in emission (§ 2.1). (*b*) The best fit parameters of the model for the longitude $l = 42°$: the terminal velocity V_T, the velocity dispersion σ_v, the centroid in z-Z_0 and the scale height σ_z are plotted as a function of the cutoff velocity V_{crit}. Emission at velocities greater than V_{crit} was modeled. This figure shows that the parameters of the model are not very sensitive to small changes in the boundaries of the region they are fit. Only the scale height shows a systematic increase. This is discussed in § 2.4.

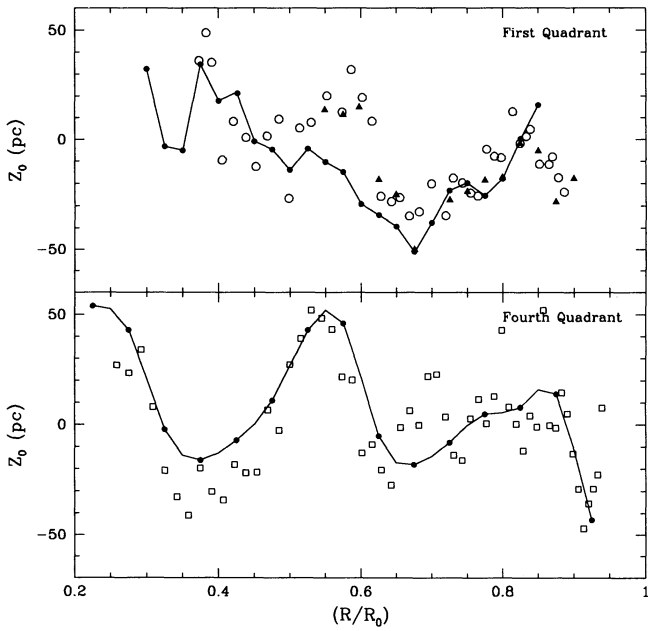

FIG. 5.—The z location of the centroid of the midplane in the first (*open circles:* Weaver & Williams survey; *triangles:* Bania & Lockman survey) and the fourth quadrant (*open squares:* Parkes survey by Kerr et al.). The solid lines are the midplane positions of the molecular gas layer as traced by CO emission (Malhotra 1994; Bronfman 1988). There is a reasonable agreement between the midplane deviations of the two phases of cold neutral gas. The midplane deviations of H I and CO differ at $l = 30°$–$37°$.

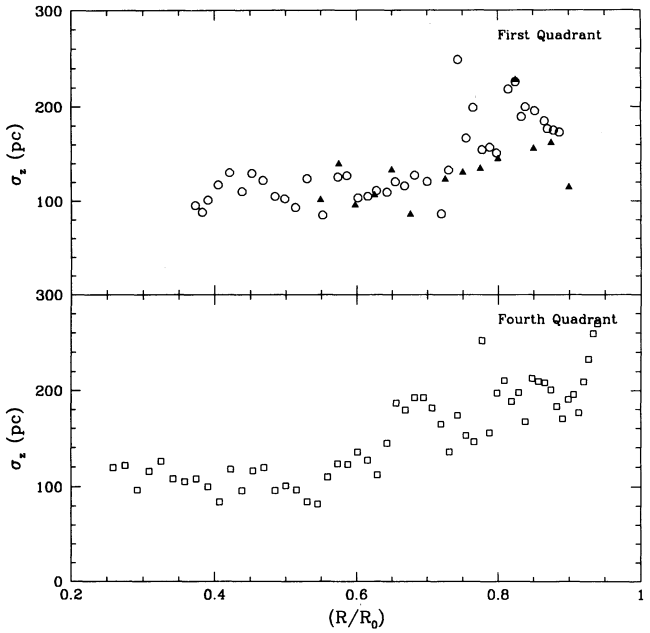

FIG. 6.—The scale heights of H I layer in the first and the fourth quadrants (*open circles*: WW survey; *triangles*: BL survey; *open squares*: Parkes survey). The H I shows similar behavior in the first and the fourth quadrants, flaring at $\simeq 0.6R_0$(5 kpc). The scale heights obtained from tangent point modeling have been corrected for broadening by the telescope beams (§ 3.2).

smaller scale height than the WW data. This is due to the limited coverage of the BL survey, combined with the increasing apparent scale height at higher longitudes as the tangent points get closer to the position of the Sun. Fitting to WW data restricted to latitude extent of the BL survey gives similar values as a fit to the BL data.

3.3. *Terminal Velocity*

In Figure 7 we show the best-fit terminal velocities for the first and the fourth quadrants. The curve for the first quadrant is compared to a similar curve derived by Gunn, Knapp, & Tremaine 1979, from the 1 K contour at the extreme velocities, after correcting for a velocity dispersion of 9 kms. The two curves agree fairly well.

There exists asymmetry between the first and the fourth quadrant terminal velocity curves. This difference is not easy to understand as a simple outward motion or as other systematic (cf: Blitz & Spergel 1991; Kerr 1962).

3.4. *Velocity Dispersion*

From Figure 8, we see that the velocity dispersion derived remains constant with radius. There are small bumps, and the scatter among neighboring points is higher than the estimated uncertainties in σ_V. The dispersion of the individual values of σ_V about the mean value is comparable to the error estimate of 1 km s^{-1}. The best linear fit to the σ_V versus R/R_0 gives the mean value of 9.2 km s^{-1} in the fourth quadrant and 9.0 km s^{-1} in the first quadrant, with a slope of $<(1/8.5)$ km s^{-1} kpc^{-1}. We recall here that this is a measurement of one-dimensional velocity dispersion in the azimuthal direction.

From the studies of face-on galaxies it is seen that the velocity dispersion of the atomic gas remains fairly constant with radius (Dickey, Hanson, & Helou 1990; Shostak & van der Kruit 1984; van der Kruit & Shostak 1982). The cooling curve of H I predicts the gas temperature to be below 10^4 K corresponding to a velocity dispersion of 10 km s^{-1}.

4. VERTICAL EQUILIBRIUM OF THE H I LAYER

Considering the condition for vertical equilibrium of the atomic gas in the galactic disk, in the simplest case of a single

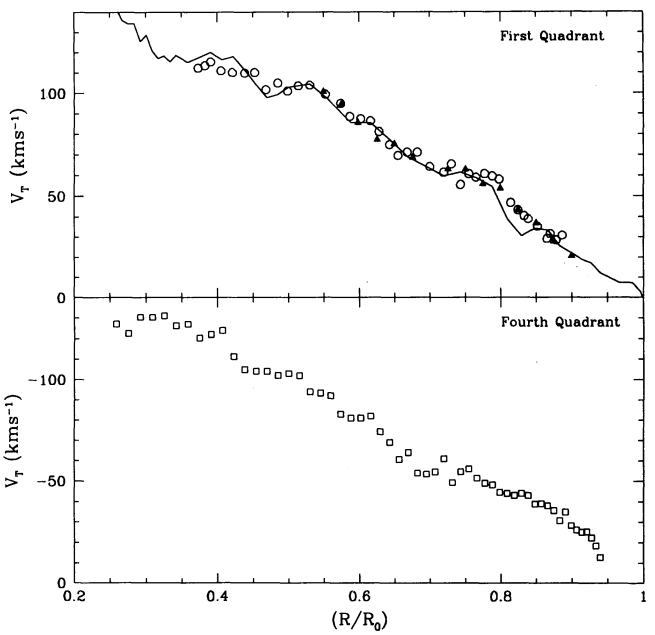

FIG. 7.—The terminal velocity V_T for the tangent point gas at different Galactic longitudes l (hence Galactic radii $R/R_0 = \sin(l)$]. The solid line shows the terminal velocity for H I from Gunn et al. 1979 (*open circles*: WW survey; *triangles*: BL survey; *open squares*: Parkes survey).

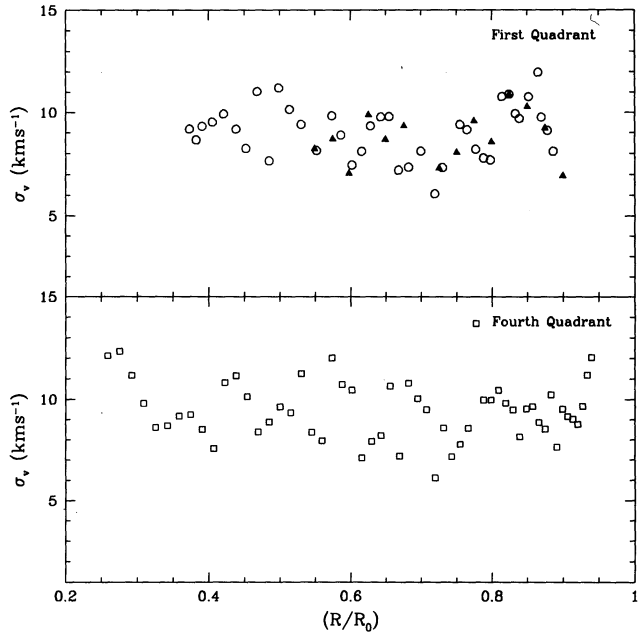

FIG. 8.—The velocity dispersion of H I as modeled from tangent point emission (*open circles*: WW survey; *triangles*: BL survey; *open squares*: Parkes survey). The velocity dispersion is seen to be fairly constant at $\simeq 9$ km s^{-1}. The scatter in the individual values and other estimates (see § 2.4) yield an uncertainty of 1 kn s^{-1} in this value.

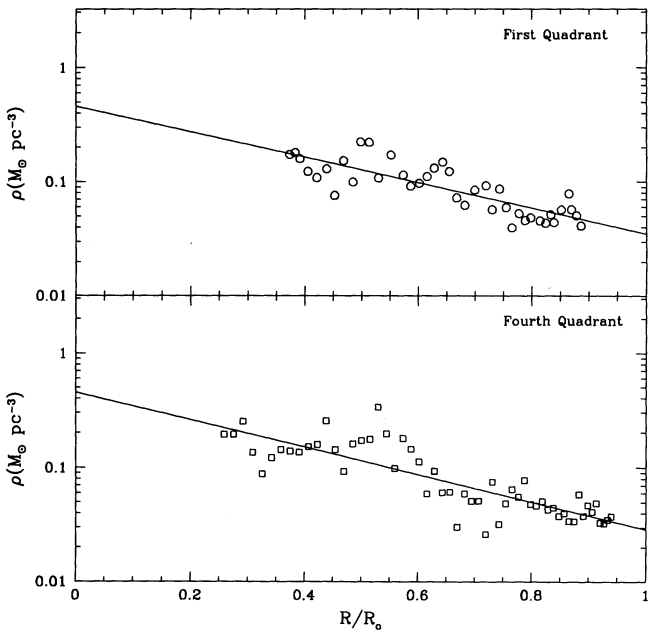

FIG. 9.—The midplane mass density of the disk $\rho_0 = \sigma_v^2/4\pi G\sigma_z^2$ (*open circles*: WW survey; *triangles*: BL survey; *open squares*: Parkes survey). Exponential disk models are fitted to the WW data in the first quadrant and Parkes data in the fourth. The best fit scalelengths are 3.4 ± 0.3 kpc and 3.1 ± 0.3 kpc for the first and the fourth quadrant, respectively. The error bars on the scalelength are calculated from bootstrapping the individual measurements of $\rho_0(R)$.

isothermal gas, the vertical component of the gravitational force is balanced by the pressure due to turbulent motions of the gas and due to magnetic fields etc.

$$K_z = -4\pi G\Sigma(z)\rho_{\rm gas}$$

$$= \frac{d}{dz}(P_{\rm kinematic} + P_{\rm magnetic} + P_{\rm cosmic\,rays} + P_{\rm radiation} \ldots). \quad (5)$$

The scope of this paper is limited to analyzing the kinematics of the H I layer and its vertical structure, so we will consider only gravitational forces on the gas and the kinetic support. Very near the plane we can assume the total disk mass density to be nearly constant ρ_0, and the surface density $\Sigma(z) = \rho_0 z$. Considering only kinematic pressure support the above equation reduces to

$$\frac{d}{dz}\rho_{\rm gas}\sigma_v^2 = -4\pi G\rho_0 z\rho_{\rm gas} \quad (6)$$

and the z-profile of the gas is a Gaussian $\rho_{\rm gas}(z) \propto \exp(-z^2/2\sigma_z^2)$ with the scale height $\sigma_z^2 = \sigma_v^2/4\pi G\rho_0$.

The total midplane mass density $\rho_0 = \sigma_v^2/4\pi G\sigma_z^2$, and is determined for each longitude, from the measurements of the scale height and the velocity dispersion, using the thin-layer approximation. We have also assumed that the velocity dispersion of H I is isotropic, so the azimuthal velocity dispersion we measure is equal to the vertical velocity dispersion. This is justified since H I is a diffuse collisional medium. Support for this assumption also comes from the isotropy of the velocity dispersion of young stars who reflect the kinematics of the parent interstellar gas (cf. Paper I). Figure 9 shows the radial profile of the midplane mass density $\rho_0(R)$ as a function of radius R for both the first and the fourth quadrants. An exponential profile (in radius) is fitted to ρ_0 measurements at each longitude and yields a scale length of 3.4 ± 0.3 kpc in the first quadrant, and 3.1 ± 0.3 kpc in the fourth.

The scale length of the midplane mass density is the same as one of measurements of the scale length of the light in the exponential disk (de Vaucouleurs & Pence 1978), suggesting a constant mass-to-light ratio at least in the inner Galaxy. There are various estimates of the scale length of our Galaxy ranging from 1.8–6 kpc (see Kent, Dame, & Fazio 1991 for a list and discussion). Most estimates from infrared studies give a scale length for the light volume density of ~ 3 kpc.

The uncertainty in the scale length of disk-mass-density is determined by the bootstrap method. This method was used because it is difficult to assign realistic error bars to each measurement of scale height σ_z and velocity dispersion σ_v (cf. previous section). Since ρ_0 depends on the square of σ_v and σ_z, the error bars on ρ_0 are even more ill-determined. We have more than 50 determinations of $\rho_0(R)$ in each of the quadrants; and the bootstrap method easily yields the uncertainty in the scale length. Each measurement involves taking the average of the gas in an interval of $\simeq 1$ kpc along the line of sight, but the measurements are separated by more than one beam width in azimuth, so we are not seeing the same parcel of gas. These points are independent apart from any correlation in the gas properties at the scale of a few hundred parsecs.

Merrifield (1992) has estimated the mass density profile of the disk to be an exponential with a scale length of ~ 5 kpc from his measurements of the scale height and assuming the velocity dispersion of the H I is 10 km s^{-1}. Using the scale height determination from the last section with $\sigma_v = 10$ km s^{-1}, gives a scale length of 4.6 kpc in the first quadrant and 3.3 kpc in the fourth. These values differ from each other and from the scale lengths calculated above using the measured σ_v and σ_z

by more than the error bar on the scale length. We may interpret this discrepancy as the true measure of the uncertainty in the scale length or as an indication that the individual measurements of σ_v and σ_z show local variations that are significant when estimating the mass density profile $\rho_0(R)$.

Extrapolating $\rho(0)$ to solar radius gives a midplane mass density of 0.03 $M_\odot$ pc^{-3}; at least a factor of $\simeq$3.5 smaller than the midplane mass density inferred at the Sun's position from stellar kinematics (which is also uncertain by a factor of 2) (Bahcall, Flynn, & Gould 1992; Bahcall 1984a, b, c; Bienaymé et al. 1987; Kuijken & Gilmore 1989a, b, c, 1991; Kuijken 1991). This implies that extra pressure is needed to support the H I layers to the observed heights.

The candidates for extra support are pressure gradients of one or more of the following: pressure due to high-velocity dispersion component(s) of the gas, magnetic pressure, cosmic ray pressure, and radiation pressure. These candidates are examined in detail by Boulares & Cox (1990) and Lockman & Gehman (1991). Given that the scale length of $\rho_0(R)$ is the same as the scale length of light in the disk, constant mass-to-light ratio of the disk is favored. The velocity dispersion of H I remains constant at 9 $\pm$ 1 km s^{-1}, showing that the decrease in $\rho_0(R)$ is reflected in the scale height of the gas, which increases with radius. This implies that the extra support for H I, whichever source it comes from, should stay constant with radius.

4.1. *Some Systematics*

We expect the H I to be in a Gaussian layer only if the gas layer is much thinner than the stellar scale height, so we may assume stellar density to be nearly constant with z. This is the approximation used in the previous sections. Now we calculate the z-profile of the atomic gas in a realistic disk potential given that it has a velocity dispersion of σ_v = 10 km s^{-1}. Forsaking the approximation that the gas is in a layer much thinner than the stellar layer, the z-profile of the gas is given by

$$\frac{d}{dz}\,\rho_{\rm gas}(z)\sigma_v^2 = -4\pi G\rho_{\rm gas}\int_0^z \rho(z')d(z')\,, \tag{7}$$

$$\frac{d^2}{dz^2}\log\,[\rho_{\rm gas}(z)] = \frac{-4\pi G}{\sigma_v^2}\,[\rho_{\rm gas}(z) + \rho_*(z) + p_{\rm molecular\ gas}(z)]\,. \tag{8}$$

The stellar distribution $[\rho_*(z)]$ is assumed to be exponential in z with a scale height of 320 pc (Bahcall & Soneira 1984), and the molecular gas profile in z is assumed to be a Gaussian with a scale height of 60 pc. The midplane mass densities of the stellar and molecular component are taken to be 0.072 $M_\odot$ pc^{-3} and 0.021 $M_\odot$ pc^{-3} respectively. H I midplane mass density is assumed to be 0.021 $M_\odot$ pc^{-3}. Figure 10 shows the z-profile for the gas in this potential.

The expected z-profile is very nearly a Gaussian with a scale height of 144 pc, but it has slightly high tails ($\sim$1.4% of the total gas lies beyond $3\sigma_z$ pc). Using this scale height and velocity dispersion of 10 km s^{-1} gives a midplane mass density 0.9 $M_\odot$ pc^{-3} as opposed to the input of 0.11 $M_\odot$ pc^{-3}. The thin-layer approximation thus leads to an underestimate of the midplane mass density by $\sim$25%.

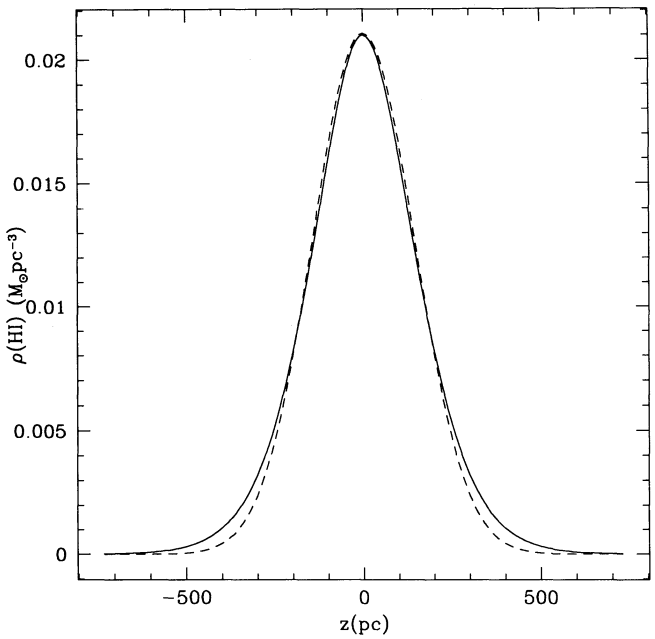

FIG. 10.—The z-profile of isothermal H I with a velocity of σ_v = 10 km s^{-1} is calculated numerically in a realistic potential: *Solid line* (cf. § 4.1). This profile has higher-than-Gaussian tails at high z; $\sim$1.4% of the gas lies beyond $3-\sigma_z$($\simeq$500 pc). The closest Gaussian profile is marked by the dashed line.

5. CONCLUSIONS AND SUMMARY

The main results of this study are as follows:

1. The velocity dispersion of H I is measured to be constant at 9 km s^{-1} across the inner Galaxy (Galactic radius of 3–8 kpc). It is also found to be constant with height above the plane.

2. The scale height of the gas increases with the Galactic radius. It increases from $\simeq$100 pc to $\simeq$220 pc going from 3 to 8 kpc in Galactic radius.

3. The midplane mass density shows an exponential decline with a scale length of 3.4 $\pm$ 0.3 kpc and 3.1 $\pm$ 0.3 kpc in the first and the fourth quadrant, respectively. Assuming that it is not a coincidence that the scale length of light in the disk is the same, this indicates a constant mass to light ratio of the disk.

4. The midplane mass density when extrapolated to solar radius, is smaller by a factor of 3.5 compared to the value derived by Kuijken & Gilmore 1989. This indicates that the H I layer needs extra support (magnetic, or cosmic-ray pressures, radiation pressure) to keep it up at the observed heights.

5. Since the exponential decline in the midplane mass density $\rho_0(R)$ with R, happens with the kinetic pressure support remaining constant, the extra support for the layer should also remain constant in the Galactic radius range of 3–8 kpc, for the M/L ratio to remain constant for the disk.

I thank G. R. Knapp for advice; and F. J. Lockman for providing the Arecibo data from the H I survey by Bania & Lockman (1984). I also thank F. J. Lockman, M. Rupen, and R. H. Lupton for discussions and R. H. Lupton for his versatile graphics package "SM." This work was supported by NSF grant AST 89-21700 to Princeton University.

REFERENCES

Badhwar, G. D., & Stephens, S. A. 1977, ApJ, 212, 494
Bahcall, J. N. 1984a, ApJ, 276, 156
———. 1984b, ApJ, 276, 169
———. 1984c, ApJ, 287, 926
Bahcall, J. N., Flynn, C., & Gould, A. 1992, ApJ, 389, 234
Bahcall, J. N., & Soneira, R. M. 1984, ApJS, 55, 67
Bienaymé, O., Robin, A., & Crézé, M. 1987, A&A, 211, 94
Bania, T. M., & Lockman, F. J. 1984, ApJS, 54, 513
Blitz, L., & Spergel, D. N. 1991, ApJ, 370, 205
Boulares, A., & Cox, D. P. 1990, ApJ, 365, 544
Bronfman, L., Alvarez, H., Cohen, R. S., & Thaddeus, P. 1989, ApJ, 324, 248
Burton, W. B. 1988, Galactic and Extragalactic Radio Astronomy (New York: Springer), 295
———. 1992, The Galactic Interstellar Medium (Berlin: Springer), 1
———. 1971, A&A, 10, 76
Celnik, W., Rohlfs, K., & Braunsfurth, E. 1979, A&A, 76, 24
de Vaucouleurs, G., & Pence, W. D. 1978, AJ, 83, 1163
Dickey, J. M., Hanson, M. M., & Helou, G. 1990, ApJ, 352, 522
Gunn, J. E., Knapp, G. K., & Tremaine, S. D. 1979, AJ, 84, 118
Jackson, P. D., & Kellman, S. A. 1974, ApJ, 190, 53
Kellman, S. A. 1972, ApJ, 175, 353
Kent, S., Dame, T. M., & Fazio, G. 1991, ApJ, 378, 131
Kerr, F. J. 1962, MNRAS, 123, 327
Kerr, F. J., Bowers, P. F., Jackson, P. D., & Kerr, M. 1986, A&AS, 66, 373
Knapp, G. R. 1987, PASP, 99, 1134
Kuijken, K. 1991, ApJ, 372, 125
Kuijken, K., & Gilmore, G. 1989a, MNRAS, 239, 571
———. 1989b, MNRAS, 239, 605
———. 1989c, MNRAS, 239, 651
———. 1991, ApJ, 367, L9
Kulkarni, S. R., & Fich, M. 1985, ApJ, 289, 792
Kwee, K. K., Muller, C. A., & Westerhout, G. 1954, Bull. Astron. Inst. Netherlands, 12, 211
Lockman, F. J. 1977, AJ, 82, 408
———. 1984, ApJ, 283, 90
Lockman, F. J., & Gehman, C. S. 1991, ApJ, 382, 182
Malhotra, S. 1994, ApJ, 433, 687 (Paper I)
———. 1994b, Ph.D. thesis, Princeton Univ.
Merrifield, M. R. 1992, AJ, 103, 1552
Mihalas, D., & Binney, J. 1981 Galactic Astronomy (New York: Freeman)
Oort, J. H. 1992, Bull. Astron. Inst. Netherlands, 6, 349
Press, W. H., Teukolsky, S. A., Vetterling, W. T., & Flannery, B. P. 1993, Numerical Recipes (Cambridge: Cambridge Univ. Press)
Rohlfs, K., & Kreitschmann, J. 1988, A&A, 201, 51
Rupen, M. P. 1990, Ph.D. thesis, Princeton Univ.
Radhakrishnan, V., & Sarma, G. 1980, A&A, 85, 249
Schmidt, M. 1957, Bull. Astron. Inst. Netherlands, 13, 247
Shane, W. W., & Bieger-Smith, G. P. 1966, Bull. Astron. Inst. Netherlands, 18, 263
Shostak, G. S., & van der Kruit, P. C. 1984, A&A, 132, 20
van der Kruit, P. C., & Shostak, G. S. 1984, A&A, 105, 351
Weaver, H., & Williams, D. R. W. 1973, A&AS, 132, 20 (WW)